Structure of the Conical Flowfield about External Axial Corners

Manuel D. Salas* and James Daywitt†
NASA Langley Research Center, Hampton, Va.

A theoretical and experimental investigation of the flowfield about symmetrical and asymmetrical external axial corners formed by the juncture of swept compressive wedges is presented. A study is made of the nature of inviscid conical cross-flow stagnation points, and the dependence of the streamline pattern on certain flow parameters is derived. The importance of imposing the physically relevant boundary condition for numerical simulations is discussed. For the asymmetrical wedge configuration, the proper boundary condition along the axial corner is shown to be a conical analog of Prandtl-Meyer flow. For the symmetrical configuration, a local solution of the irrotational equations is obtained. The solution is shown to be applicable to cones and internal and external corners. For symmetrical internal corners, the solution is unique; the corner is a nodal point of streamlines. The possible multiple solutions for external corners and cones are discussed. Further insight into the flow structure is revealed by the experimental results. The consistency of the derived flow models with the Euler limit of the Navier-Stokes equations is substantiated by the experimental data.

I. Introduction

EXTERNAL corner configurations, such as depicted in Fig. 1, are representative of geometric features found on supersonic and hypersonic aircraft. The prediction of loads due to the flow about external corners formed, for example, at engine inlets and wing tips is important for both component and overall vehicle design. Also of interest is the influence of external corner interference effects on control surfaces, on aftbody flows, and on the plume flowfield of nonaxisymmetric nozzles. Yet there have been few, if any, experimental studies of external corner flows. Although several inviscid theoretical investigations[1-6] of the corner and related problems have been undertaken, their applicability is necessarily limited by the assumptions required to linearize the governing equations. Furthermore, none of these studies has dealt with the nature of the cross-flow stagnation point(s) that are present in an inviscid, conical flowfield.

Recently, however, the first numerical results for the nonlinear inviscid flowfield about external corners have been presented by Kutler and co-workers.[7,8] Unfortunately, despite being solutions of the fully nonlinear equations, these numerical results may not reflect the actual physics, particularly in the limit of infinite Reynolds number. In this paper it is proposed that these mathematically admissible solutions are a consequence of imposing boundary conditions based on a flow model that is not physically justifiable. To support this assertion and to obtain further insight into the structure of the flowfield about external corners, the results of an experimental study are presented. The main theme of the paper is the development of a new inviscid flow model based upon an analysis of the governing equations in the neighborhood of the external corner. The effect of finite Reynolds number on the new model is inferred from the experimental results.

Presented as Paper 78-59 at the AIAA 16th Aerospace Sciences Meeting, Huntsville, Ala., Jan. 16-18, 1978; submitted March 6, 1978; revision received July 5, 1978.

Index categories: Computational Methods; Supersonic and Hypersonic Flow; Transonic Flow.

*Aero-Space Technologist, Supersonic Aerodynamics Branch, High-Speed Aerodynamics Division. Member AIAA.

†Visiting Scientist, Institute for Computer Applications in Science and Engineering; presently Engineer, Aerothermodynamics, Re-entry and Environmental Systems Division, General Electric Company, Philadelphia, Pa. Member AIAA.

II. Flowfield Description

The external axial corners considered in this study are formed by the juncture of swept compressive wedges. The axial corner, as defined in Fig. 1, is the line of intersection of the wedge surfaces. The wedges are assumed to be infinite in extent so that no characteristic length exists. The inviscid supersonic flowfield is thus conically self-similar with the conical origin at the intersection of the wedge leading edges. The cross-flow plane, illustrated in Fig. 2, is formed by projecting the flowfield onto the surface of a unit sphere centered at the conical origin and then projecting this surface onto a plane. The projection of the velocity vector onto the spherical surface defines the cross-flow velocity. The cross-flow plane is divided into three regions separated by cross-flow sonic lines. The cross-flow hyperbolic regions I and II in Fig. 2 are the known two-dimensional wedge flows corresponding to effective wedge angles $\delta_{1,2} = \arctan(\tan\delta_{1,2}/\cos\Lambda_{1,2})$ facing a freestream velocity component $V_{1,2} = V_\infty \cos\Lambda_{1,2}$. Region III is elliptic in the cross-flow plane. The region is bounded by the corner segment of each wedge surface, by an unknown peripheral bow shock, and by the known cross-flow sonic lines. The sonic lines trace the intersection of the Mach cone emanating from the conical apex with each of the two-dimensional wedge shock layers.

The occurrence of at least one vortical singularity (a cross-flow stagnation point formed as a nodal point of streamlines at which the entropy, density, and spherical radial velocity are multivalued) in region III may be presupposed based on the following observations. The cross-flow velocity on the wedge surface at the region III sonic line boundaries is always directed toward the corner. The surface streamlines from regions I and II carry their respective two-dimensional wedge entropy values. At the bow shock in region III, the cross-flow streamlines are directed inward. The entropy carried by the bow shock streamline that wets the body surface will differ from the wedge values. Thus, even for symmetrical wedges, a vortical singularity must appear.

III. Kutler-Shankar Model

The numerical solutions in Ref. 8, for symmetrical configurations, indicate a surface streamline pattern as sketched in Fig. 3a. The axial corner thus appears as a saddle line in this flow model. The corresponding streamline behavior in the cross-flow plane projection is shown in Fig. 3b. Since the streamlines that diverge from the corner (Fig. 3) carry an

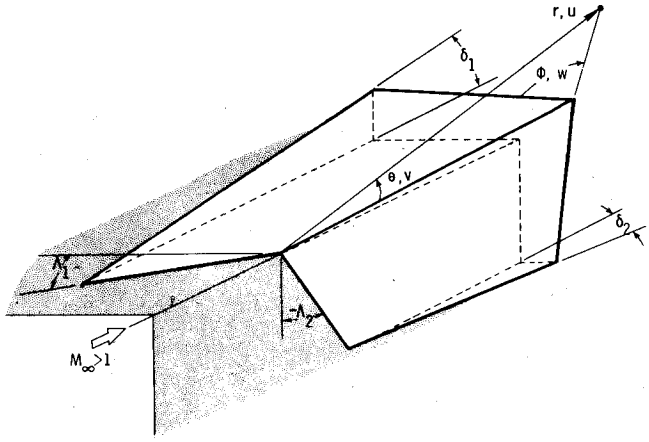

Fig. 1 Geometry of the conical external axial corner.

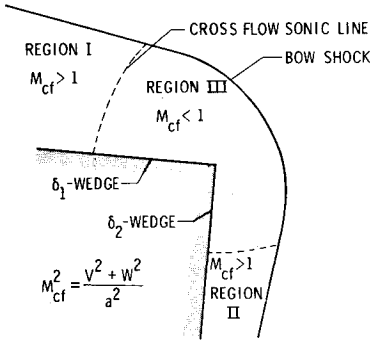

Fig. 2 Cross-flow plane hyperbolic and elliptic regions.

entropy value from the curved portion of the bow shock, a nodal cross-flow stagnation streamline (vortical singularity) must exist on each wedge surface.

Figures 3c and 3d show the surface and cross-flow streamline patterns for the asymmetrical case arising from the numerical solutions in Ref. 8. The picture is altered from the symmetrical case in that the vortical singularities now are located at unequal distances from the axial corner. Thus, the only influence of the asymmetrical wedge arrangement is to introduce a skewness into the symmetrical wedge flow pattern.

The flow structure appearing in a numerical solution is dependent upon the imposed boundary conditions. In particular, the key feature that distinguishes the external corner problem is the treatment of the surface tangency condition on each wedge at the corner. A premise of the Kutler-Shankar model is that the axial corner is a streamline in both the symmetrical and asymmetrical arrangements. The boundary condition is enforced along the corner by simultaneously requiring the vanishing of the velocity component normal to each wedge surface. The same boundary condition also has been suggested in Ref. 9.‡ However, as will be shown in Sec. IV of this paper, the axial corner cannot be a streamline for asymmetrical configurations.

For the symmetrical wedge case, the results obtained in Ref. 8 do not place the vortical singularity at the corner point. Instead, the entropy at the corner is single-valued and set equal to that at the weakest portion of the bow shock. An alternative corner treatment, which places a vortical singularity at the corner, is discussed in Sec. V.

IV. Corner Boundary Condition: Asymmetrical Case

Consider a spherical frame with its origin at the conical origin and its axis along the axial corner, as in Fig. 1. After

‡A similarly arbitrary boundary condition was imposed in Ref. 10. It was recognized, however, that the tangency condition on each side of the surface discontinuity did not have to be satisfied simultaneously.

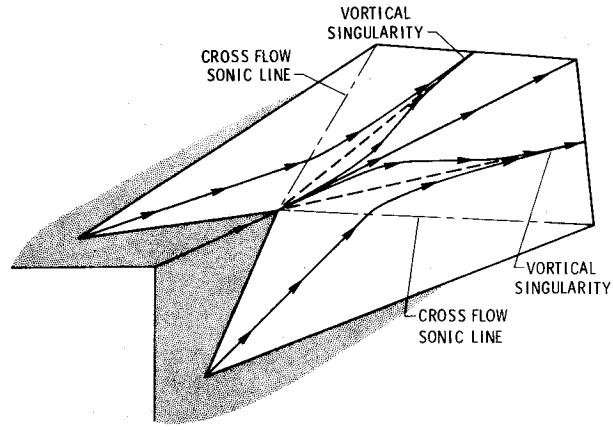

a) Surface streamlines: symmetric configuration

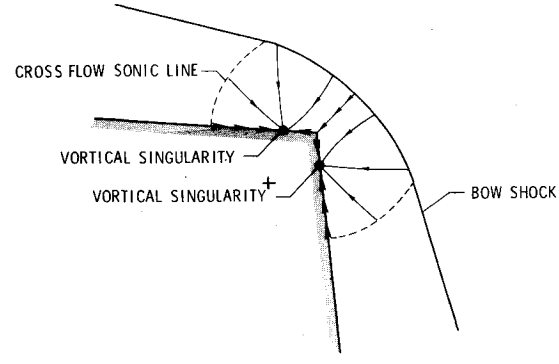

b) Cross-flow streamlines: symmetric configuration

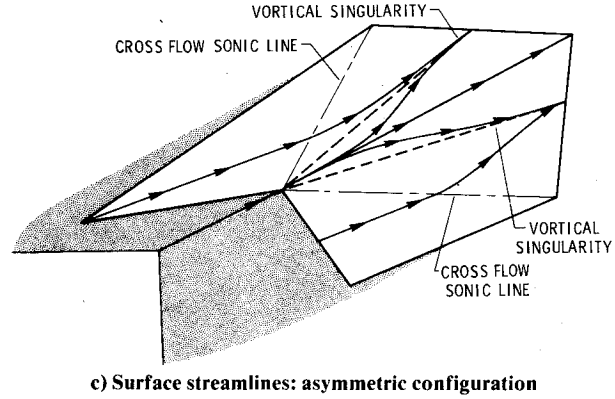

c) Surface streamlines: asymmetric configuration

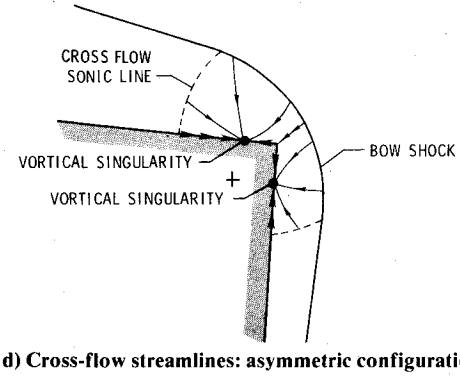

d) Cross-flow streamlines: asymmetric configuration

Fig. 3 External axial corner inviscid flow model.[8]

taking into consideration the conical nature of the problem, the governing equations on the unit sphere are

$$v\rho_\theta + \frac{w\rho_\phi}{\sin\theta} + \rho\left(v_\theta + \frac{w_\phi}{\sin\theta} + 2u + v\cot\theta\right) = 0 \qquad (1a)$$

$$v v_\theta + \frac{w v_\phi}{\sin\theta} + \frac{p_\theta}{\rho} + uv - w^2\cot\theta = 0 \tag{1b}$$

$$v w_\theta + \frac{w w_\phi}{\sin\theta} + \frac{p_\phi}{\rho\sin\theta} + uw + vw\cot\theta = 0 \tag{1c}$$

$$v u_\theta + \frac{w u_\phi}{\sin\theta} - (v^2 + w^2) = 0 \tag{1d}$$

$$v S_\theta + \frac{w S_\phi}{\sin\theta} = 0 \tag{1e}$$

where u, v, and w are the velocity components in the r, θ, and ϕ directions, respectively, and p, ρ, and S denote pressure, density, and entropy, respectively. To obtain a set of equations valid at the corner, Eqs. (1) are multiplied by θ and the limit as $\theta \to 0$ is taken,[11] which yields

$$w\rho_\phi + \rho(w_\phi + v) = 0 \tag{2a}$$

$$\rho w(v_\phi - w) = 0 \tag{2b}$$

$$\rho w(w_\phi + v) + p_\phi = 0 \tag{2c}$$

$$w u_\phi = 0 \tag{2d}$$

$$w S_\phi = 0 \tag{2e}$$

Using the definition of entropy

$$S = \ell n p - \gamma \ell n \rho \tag{3}$$

in Eqs. (2) shows that, at $\theta = 0$,

$$(w^2 - a^2)(w_\phi + v) = 0 \tag{4}$$

where a is the speed of sound. It is concluded, therefore, that two solutions are possible at the corner. Equation (4) must hold for all values of the meridional angle ϕ in the range $0 \le \phi \le \Phi$, where Φ is the exterior angle formed by the two wedge surfaces. The solution $w_\phi + v = 0$ corresponds to a cross-flow stagnation point at the corner and will be considered in detail in Sec. V. The solution

$$w^2 = a^2 \tag{4a}$$

leads to the conical analog of Prandtl-Meyer flow. Equation (4a) is valid within the Prandtl-Meyer fan, which extends from the perpendicular to the oncoming cross-flow direction on the high-pressure wedge surface to the cross-flow Mach angle for which the cross flow becomes parallel to the low-pressure wedge. Outside this range, the vector rotation $w_\phi = -v$ in Eq. (4) is satisfied.

The proposed flow pattern for the asymmetrical case is presented in Figs. 4a and 4b. The significant feature is that, unlike the numerical model in Ref. 8 (Figs. 3c and 3d), the flow "spills" over the axial corner. In the asymmetrical model in Fig. 4, the corner is considered a surface discontinuity line requiring the satisfaction of the tangency condition on each wedge separately. For an inviscid fluid, the subsonic cross-flow velocity approaching the corner will accelerate to sonic speeds.[12] In a numerical formulation, the corner point is multivalued and determined by expansion jump conditions.

Assuming that the cross-flow direction is from left to right, as shown in Fig. 4, and denoting by p_*, ρ_*, S_*, and u_* the values of the pressure, density, entropy, and radial velocity component just ahead of the corner, then it can be shown by integrating Eq. (2b), with the help of Eq. (4a) and Bernoulli's equation, that at the corner, within the Prandtl-Meyer fan,

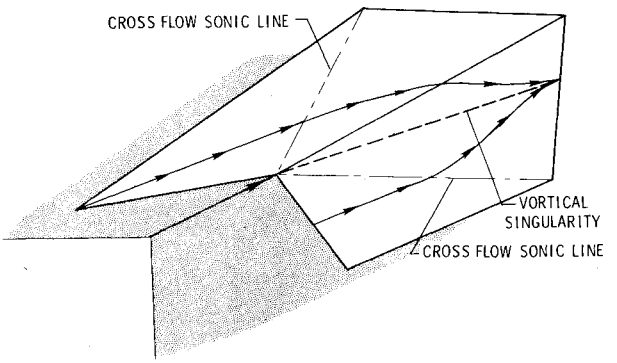

a) Surface streamlines: asymmetric configuration

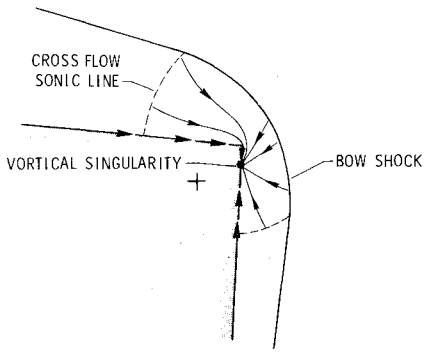

b) Cross-flow streamlines: asymmetric configuration

Fig. 4 Proposed external axial corner inviscid flow model: asymmetric case.

the flow variable are given by

$$v = \sqrt{q_{\max}^2 - u_*^2}\ \sin\left(\sqrt{\frac{\gamma-1}{\gamma+1}}\,\omega\right) \tag{5a}$$

$$w = \sqrt{\frac{\gamma-1}{\gamma+1}}\sqrt{q_{\max}^2 - u_*^2}\cos\left(\sqrt{\frac{\gamma-1}{\gamma+1}}\,\omega\right) \tag{5b}$$

$$\frac{p}{p_*} = \left[\cos\left(\sqrt{\frac{\gamma-1}{\gamma+1}}\,\omega\right)\right]^{2\gamma/(\gamma-1)} \tag{5c}$$

$$\frac{\rho}{\rho_*} = \left[\cos\left(\sqrt{\frac{\gamma-1}{\gamma+1}}\,\omega\right)\right]^{2/(\gamma-1)} \tag{5d}$$

$$S = S_* \tag{5e}$$

$$u = u_* \tag{5f}$$

where the angle ω is measured from the perpendicular to the oncoming cross-flow direction. In this case, ω is defined by $\omega = \phi - (\pi/2)$. These equations are the same as for a two-dimensional Prandtl-Meyer expansion[13] except that the maximum adiabatic velocity ($q_{\max}$) is reduced by the radial velocity component u_*. The usual Prandtl-Meyer relation between the flow inclination ν and Mach number is now given by

$$\nu = -\sqrt{\frac{\gamma-1}{\gamma+1}}\arctan\left(\sqrt{\frac{\gamma-1}{\gamma+1}}\sqrt{M_{cf}^2 - 1}\right) + \arctan\left(\sqrt{M_{cf}^2 - 1}\right) \tag{6}$$

where M_{cf} is the cross-flow Mach number.

The sonic line originating at the corner can be shown to be perpendicular to the oncoming flow.[13] This sonic line forms a bubble of supersonic cross flow near the corner (Fig. 5) which

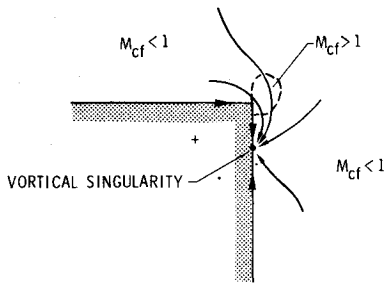

Fig. 5 Corner detail: asymmetric configuration.

could terminate with a cross-flow shock ahead of the cross-flow stagnation point. However, depending upon the flow conditions, the deceleration from a supersonic to subsonic cross-flow speed could be brought about smoothly without a shock, since the cross-flow velocity is not coupled directly to the pressure through Bernoulli's equation.[14]

V. Flow Structure near the Symmetrical Corner

Along the wedge surface ($\phi=0$) and along the symmetry plane ($\phi=\Phi/2$), the governing equations [Eqs. (1)] take the simple form

$$\left(1-\frac{v^2}{a^2}\right)v_\theta+\left(2-\frac{v^2}{a^2}\right)u=-\frac{(v\cos\theta+w_\phi)}{\sin\theta} \tag{7a}$$

$$P_\theta=-\gamma v(u+v_\theta)/a^2 \tag{7b}$$

$$P_\phi=0 \tag{7c}$$

$$v=u_\theta \tag{7d}$$

$$vS_\theta=0 \tag{7e}$$

where, for convenience, the pressure has been replaced by the natural logarithm of pressure P.

Since the flow is symmetrical about the corner, the corner must be a cross-flow stagnation point. Studies of cross-flow stagnation points in conical flows (see, for example, Refs. 15 and 16) have shown that the streamline patterns are related directly to the types of pressure extrema. Therefore, at a cross-flow stagnation point anywhere along the wedge surface or the symmetry plane, the streamline patterns are governed by the determinant of the Hessian matrix (henceforth referred to as the Hessian),

$$\Delta=P_{\theta\theta}P_{\phi\phi}-P_{\theta\phi}^2 \tag{8}$$

since both P_θ and P_ϕ are zero.

If $\Delta>0$, the stagnation point is a streamline saddle point; if $\Delta<0$, then it is a streamline nodal point. If the Hessian is identically zero, additional information is required to establish its nature.

By differentiating Eqs. (1), it can be shown that the Hessian may be written as

$$\Delta=\gamma^2M_0^4\xi(1+\xi)^2(2+\xi)\sin^2\theta \tag{9}$$

Where $M_0=u/a$ and $\xi=v_\theta/u$, with the subscript 0 denoting cross-flow stagnation conditions. The behavior of Δ with ξ is shown in Fig. 6. If the stagnation point is located at the axial corner ($\theta=0$), the indeterminate case, $\Delta=0$, results.

The vanishing of the Hessian at the corner necessitates a local analysis of the Euler equations near the corner. However, since the fully nonlinear equations are not amenable to analysis, the problem is simplified by assuming isentropic flow. This assumption is not expected to be a severe limitation, since it has been shown to provide a good qualitative description of cross-flow stagnation points, even for strongly rotational flows.[15,16]

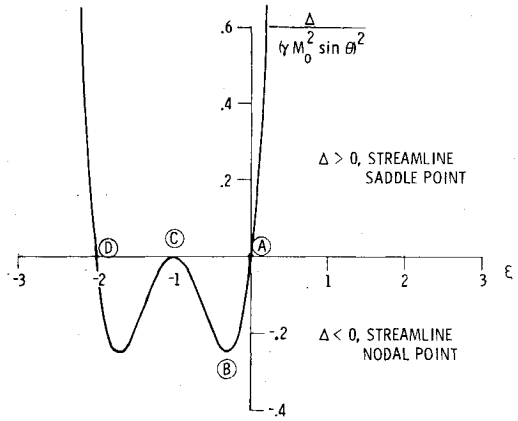

Fig. 6 The Hessian, $\Delta=P_{\theta\theta}P_{\phi\phi}-P_{\theta\phi}^2$, at a cross-flow stagnation point ($\theta>0$).

Assuming, then, isentropic flow, a conical potential $rF(\theta,\phi)$, can be defined which, on the unit sphere and in the neighborhood of $\theta=0$, satisfies the equation[12]

$$F_{\theta\theta}+(1/\theta)F_\theta+(1/\theta^2)F_{\phi\phi}+2F=0 \tag{10}$$

with the velocity components given by

$$u=F,\quad v=F_\theta,\quad w=(1/\theta)F_\phi \tag{11}$$

The boundary conditions that a solution to Eq. (10) must satisfy are

$$u=u_0 \quad \text{at } \theta=0 \tag{12a}$$

$$w=0 \quad \text{at } \phi=0,\Phi/2 \tag{12b}$$

By separation of variables, the solution is found to be

$$F(\theta,\phi)=\sum_n^\infty C_n\cos(2n\epsilon\phi)J_\kappa(\sqrt{2}\theta) \tag{13}$$

where

$$\epsilon=\pi/\Phi,\quad \kappa=2n\epsilon,\quad n=0,1,2,3,\ldots$$

and where $C_0=u_0$ and the C_n's for $n>0$ are undetermined constants. J_κ represents a Bessel function of the first kind of order κ.

From Eqs. (13) and (11), the leading terms in the expansion for the velocity components, near $\theta=0$, are§

$$u=u_0\left(1-\frac{\theta^2}{2}\right)+\frac{C_1}{(2\epsilon)!}\cos(2\epsilon\phi)\left(\frac{\sqrt{2}\theta}{2}\right)^{2\epsilon}+\ldots \tag{14a}$$

$$v=-u_0\theta+\frac{\epsilon\sqrt{2}C_1}{(2\epsilon)!}\cos(2\epsilon\phi)\left(\frac{\sqrt{2}\theta}{2}\right)^{2\epsilon-1}+\ldots \tag{14b}$$

$$w=-\frac{\epsilon\sqrt{2}C_1}{(2\epsilon)!}\sin(2\epsilon\phi)\left(\frac{\sqrt{2}\theta}{2}\right)^{2\epsilon-1}+\ldots \tag{14c}$$

and, from Bernoulli's equation and the isentropic relation, the pressure is given by

$$p=p_0+\rho_0\left\{u_0C_1\frac{(2\epsilon-1)}{(2\epsilon)!}\cos(2\epsilon\phi)\left(\frac{\sqrt{2}\theta}{2}\right)^{2\epsilon}-\left(\frac{C_1\epsilon}{(2\epsilon)!}\right)^2\left(\frac{\sqrt{2}\theta}{2}\right)^{4\epsilon-2}\right\}+\ldots \tag{14d}$$

§In Eqs. (14) if 2ϵ is not an integer then the factorial is defined in terms of the Gamma function $(2\epsilon)!=\Gamma(2\epsilon+1)$.

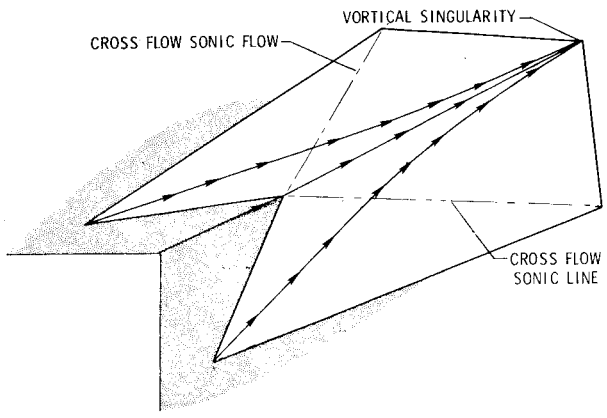

a) Surface streamlines: symmetric configuration

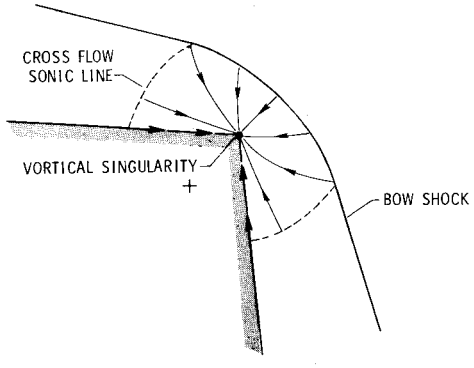

b) Cross-flow streamlines: symmetric configuration

Fig. 7 Inviscid corner flow model with nodal singularity at the corner: symmetrical case.

Since v vanishes at the cross-flows stagnation point, the character of the singularity can be determined from the value of v_θ,

$$v_\theta = -u_0 + C_I \frac{(2\epsilon-1)\epsilon}{(2\epsilon)!}\cos(2\epsilon\phi)\left(\frac{\sqrt{2}\theta}{2}\right)^{2\epsilon-2} + \ldots \qquad (15)$$

in the limit of $\theta \to 0$. The flow at the corner is, thus, strongly dependent on the exterior angle ($\Phi = \pi/\epsilon$) and in certain cases on the value of the constant C_I. For internal corners, $\infty > \epsilon > 1$, the corner is a nodal point of streamlines, independent of the value of C_I, since $v_\theta = -u_0$ for all values of ϕ. For a flat plate or a cone,[17] $\epsilon = 1$, the cross-flow stagnation point is a node or a saddle of streamlines, depending on the value of C_I. The constant C_I remains undetermined in the present local analysis but can be evaluated from a global solution. For example, by matching the present solution with the linear solution for a cone developed in Ref. 16,

$$C_I = (4\tilde{\alpha} - 2)u_0 \qquad (16)$$

where $\tilde{\alpha}$ is the ratio of angle of attack to the cone half-angle.

An important fact to observe is that an analysis of sharp corners performed as a limiting process of a rounded corner with vanishing radius of curvature must fail in some neighborhood of the corner, since, for a rounded corner, the significant parameter ϵ remains equal to unity throughout the limiting process.

For external corners, $\frac{1}{2} < \epsilon < 1$, any finite value of the undetermined constant C_I produces a saddle of streamlines at the corner with a weak singularity in v and, in the range $\frac{1}{2} < \epsilon < \frac{3}{4}$, also a weak singularity in p. The singularity in p appears as a cusp in the pressure distribution at the corner. Since this behavior in the pressure distribution is not predicted by the global linear solution,[6] it must indicate either a breakdown of the linear solution at the corner or that the undetermined constant C_I is zero. If C_I is zero, then the corner is a node of streamlines, and a matching of the global solution with the local analysis is achieved. This alternative flow model is shown in Fig. 7.

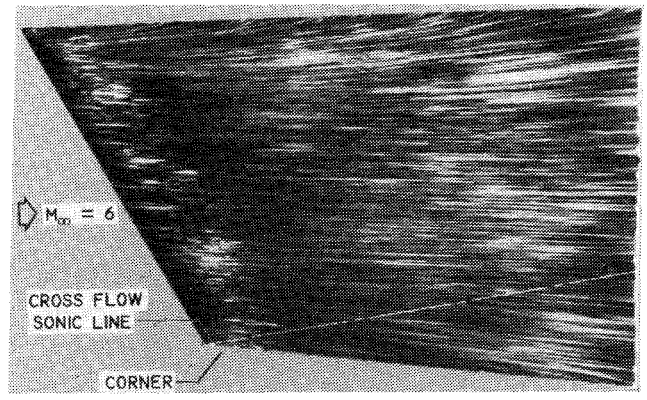

a) High-pressure wedge (face 1)

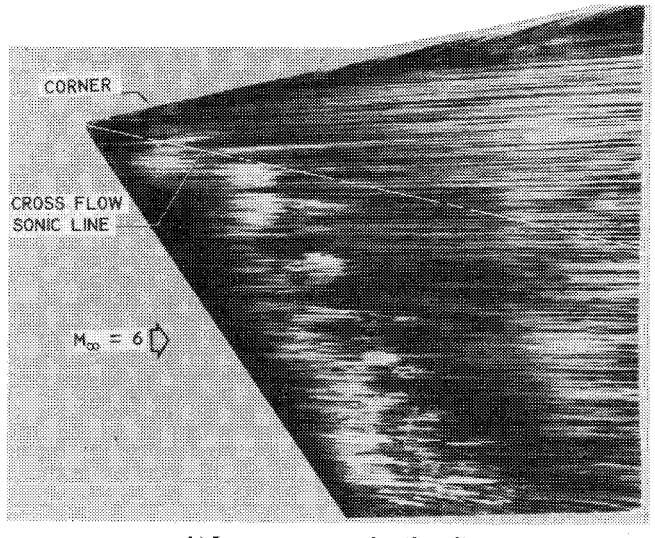

b) Low-pressure wedge (face 2)

Fig. 8 Oil streaklines on asymmetrical model (R_e/cm = 6.07×10^5, $\Lambda_1 = 30$ deg, $\Lambda_2 = 30$ deg, $\delta_1 = 10$ deg, $\delta_2 = 5$ deg).

VI. Transition

Thus far, two distinct flow behaviors at the corner have been described. One characteristic of asymmetrical configurations permits the flow to spill over the corner; the other, characteristic of symmetrical configurations, exhibits a cross-flow stagnation point at the corner. In the second case, the cross-flow stagnation point has been shown to be either a saddle or nodal point of streamlines. Clearly, the question arises as to how the transition from the spillover pattern to the stagnation-point pattern occurs. An investigation of the transition process should consider whether transition occurs smoothly or discontinuously, or through a series of intermediate flow patterns. This investigation, although very important, is beyond the scope of the present paper.

VII. Experimental Result

The use of experimental data to resolve questions about the inviscid flow pattern is strictly limited by viscous effects. The existence of streamline nodal point singularities requires the assumptions of both conical and inviscid flow. Nevertheless, experimental measurements of flowfields about cones[18] have shown that, where the inviscid flow structure dominates, a viscous counterpart of a vortical singularity can be determined. For the external corner problem, some qualitative

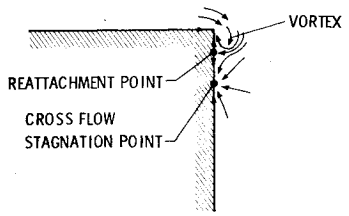

Fig. 9 Sketch of cross-flow stagnation point and vortex on face 2 of the asymmetric model.

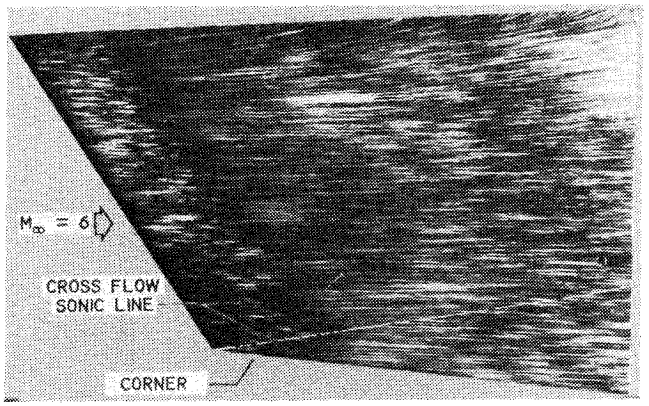

a) Face 1

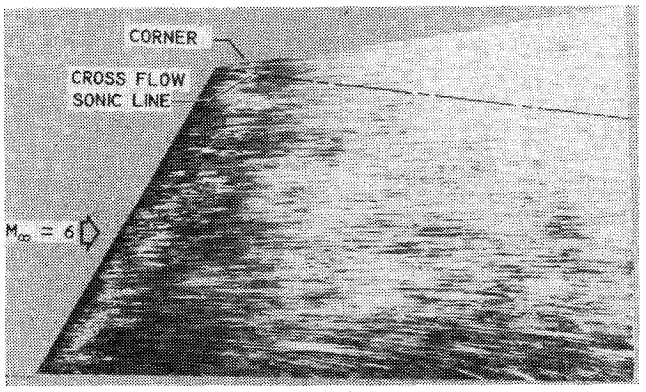

b) Face 2

Fig. 10 Oil streaklines on symmetrical model ($R_e/\text{cm} = 6.07 \times 10^5$, $\Lambda_1 = \Lambda_2 = 30$ deg, $\delta_1 = \delta_2 = 10$ deg).

features of the inviscid flow pattern should be discernable from experimental results. Thus, a flow visualization study was conducted in the NASA Langley 50.8-cm hypersonic blowdown tunnel. Two models were tested, each with leading edges meauring 22.5 cm and with an axial corner 26 cm long. The defining angles (Fig. 1) for the asymmetrical model where $\Lambda_1 = 30$ deg, $\Lambda_2 = -30$ deg, $\delta_1 = 10$ deg, and $\delta_2 = 5$ deg; for the symmetrical model, $\Lambda_1 = \Lambda_2 = 30$ deg and $\delta_1 = \delta_2 = 10$ deg. The flow test conditions were $M_\infty = 6$ and Reynolds number per centimeter of 6.07×10^5.

The photograph in Fig. 8a of the asymmetrical model shows the oil-flow streaklines on the high-pressure wedge (face 1). The streaklines in this, and in all experimental photographs, confirm that the conical nature of the inviscid flow is preserved.

The streaklines in Fig. 8a clearly indicate that, as in the proposed inviscid model (Figs. 4a and 4b) and in contrast to the numerical results (Figs. 3c and 3d), the flow is toward the axial corner. This pattern is even more pronounced on the freestream edge (upper portion of Fig. 8a), where the pressure differential is greater.

The lower-pressure wedge (face 2) of the asymmetrical model cannot be expected to resemble the inviscid flow pattern near the corner. Instead, a vortex is shed in a viscous fluid encountering such a sharp expansion turn.[12] From the streakline pattern appearing in Fig. 8b, and through a close examination of vapor screen photographs, an interpretation

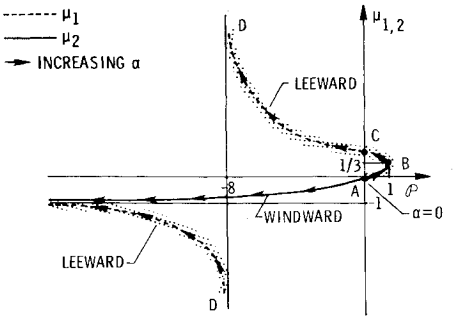

a) Exponent locus for streamlines at a cross-flow stagnation point ($\theta > 0$)[15]

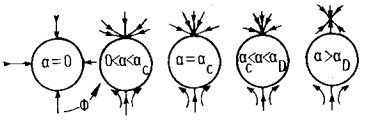

b) Streamline patterns on a cone with increasing angle of attack α

Fig. 11 Structure of the flowfield about circular cones.

of the flowfield near the corner has been constructed. A sketch of the conjectured flowfield is presented in Fig. 9.

The oil-flow streaklines on the symmetrical wedge model are pictured in Figs. 10a and 10b. Near the axial corner, the streaklines are almost coincident with conical rays. Upon magnification of the corner region, a very small cross-flow component directed away from the corner can be detected. This result thus supports the inviscid model, which places a cross-flow saddle point at the corner (Figs. 3a and 3b). However, the analysis presented in Sec. V has shown that the slightest rounding of the corner may produce a cross-flow streamline pattern that does not correspond to a truly sharp corner. Thus, even weak viscous effects at the corner could predominate over the inviscid pattern. Therefore, no definite conclusion can be drawn for this case.

The effects of yaw and angle of attack, representing additional asymmetrical configurations, also have been investigated. These results, which show the features already discussed for the asymmetrical model, will be collected in a forthcoming report.

VIII. Some Observations About the Cone

Historically, an understanding of the structure of conical flows has evolved primarily from studies devoted to cones. This present study of the corner problem, of which the cone may be viewed as a special case, has introduced a parameter Δ [Eq. (8)] that can be used to shed some light on previous conclusions about the behavior of cross-flow stagnation points on a cone at angle of attack.

For a circular cone, Melnik[15] found that the exponent $\mu_{1,2}$ governing the locus of streamlines near a cross-flow stagnation point behaves as shown in Fig. 11a, with the singular behavior at $\mathcal{P} = -8$ signalling the liftoff of the vortical singularity. However, since the $\mu = \mu_{1,2}$ curve is multivalued, the possibility remained that the vortical singularity could move circumferentially away from the leeward symmetry plane following a local minimum in surface pressure. In later studies, it was recognized that Melnik's parameter $\mathcal{P} \sim P_{\phi\phi}$ is not sufficient to establish the streamline behavior. Bakker and Bannink,[16] for example, mentioned the need to somehow include variation of P in the θ direction in the prediction of the streamline pattern. They proceeded to establish the streamline pattern by using results from linearized theory. The results that they obtained can, however, be prediced without appealing to linearized theory.

The required parameter to account properly for pressure variations in both the ϕ and θ directions is the Hessian, as given by Eq. (9). For the circular cone, θ is the cone half-angle and $\xi = w_\phi/(u \sin\theta)$. With the Hessian plotted in Fig. 6, it is evident that the various segments of Fig. 11a form two

branches corresponding to the windward and leeward symmetry planes, with points A through D indicating the same flow conditions in Figs. 6 and 11. A cone at zero angle of attack corresponds to point A. As the angle of attack is increased, the streamline pattern at the stagnation point on the leeward side changes from A to B to C until eventually liftoff occurs at D (see Fig. 11b). With a further increase in angle of attack, the leeward curve in Fig. 11a approaches the $\mu_1 = -1$ asymptote from below. At the same time, as the angle of attack increases, the stagnation point on the windward symmetry plane remains a saddle point that asymptotically approaches $\mu_2 = -1$ from above (see Fig. 11a).

When the streamline patterns, as sketched in Fig. 11b, are considered simultaneously with the Hessian behavior in Fig. 6, it follows that at liftoff the leeward cross-flow stagnation point cannot move away from the symmetry plane, since this will require an abrupt change in the sign of ξ or a switch in the character of the cross-flow stagnation point on the windward side, neither of which is consistent with Figs. 6 and 11.

IX. Conclusions

A flow model for the conical external corner was developed. It was shown that the proper boundary condition for the asymmetrical case is a conical analog of Prandtl-Meyer flow with cross-flow sonic conditions at the corner.

For the symmetrical case, the conical flowfield structure was shown to be governed by the nature of the corner cross-flow stagnation point. The relations for the pressure extremum, from which the streamline pattern follows, were shown to be indeterminate at the corner. An alternate analytical approach, valid in the neighborhood of the corner, was developed to resolve the qualitative flow structure. Applied to cones, the approach was shown to match with other analytical methods. Internal corners were found to be streamline nodal points. The method, applied to external corners, showed the possible existence of multiple solutions.

Flow visualization experiments confirmed the asymmetrical model. For the symmetrical corner, further experimental studies are needed to understand fully the flow behavior near the corner. The study was able to give a new interpretation to the pioneering work of Melnik and indicates that, in the case of a cone, the vortical singularity remains in the symmetry plane.

Finally, it has been demonstrated that the importance of boundary conditions should not be underestimated. As Moretti[19] has stated, a "... problem is defined only when a proper set of initial and/or boundary conditions is given. The boundary conditions are such an important part of the definition of a problem that the patterns of two flowfields can be completely different from one another because of some differences in the flow boundaries, despite the fact that both flows obey the same system of indefinite partial differential equations."

Acknowledgment

This work was supported in part by NASA Contract No. NAS1-14101.

References

[1]Lagerstrom, P. A. and Van Dyke, M. D., "General Considerations About Planar and Non-Planar Lifting Systems," Douglas Aircraft Co., Santa Monica, Calif., SM-13432, June 1949.

[2]Hillier, R., "The Effects of Yaw on Conical Wings at High Supersonic Speeds," *The Aeronautical Quarterly*, Vol. XXI, Pt. 3, Aug. 1970, pp. 199-210.

[3]Woods, B. A., "Hypersonic Flow with Attached Shock Waves over Delta Wings," *The Aeronautical Quarterly*, Vol. XXI, Pt. 4, Nov. 1970, pp. 379-399.

[4]Pike, J., "The Pressure on Flat and Anhedral Delta Wings with Attached Shock Waves," *The Aeronautical Quarterly*, Vol. XXIII, Pt. 4, Nov. 1972, pp. 253-262.

[5]Ferri, A., Dash, S., and Del Guidice, P., "Methodology for Three Dimensional Nozzle Design," Advanced Technology Lab., Westbury, N.Y., ATL TR 195; also available as NASA CR-132438.

[6]Vorob'ev, N. F. and Fedosov, V. P., "Supersonic Flow Around a Dihedral Angle (Conical Case)," *Fluid Dynamics*, Vol. 7, July 1974, pp. 852-856,

[7]Kutler, P., Shankar, V., Anderson, D. A., and Sorenson, R. L., "Internal and External Axial Corner Flows. Aerodynamic Analyses Requiring Advanced Computers, Pt. I," NASA SP-347, March 1975, pp. 643-658.

[8]Kutler, P. and Shankar, V., "Computation of the Inviscid Supersonic Flow Over an External Axial Corner," *Proceedings of the 1976 Heat Transfer and Fluid Mechanics Institute*, Davis, Calif., June 21-23, 1976, pp. 356-373.

[9]Prozan, R. J., Spradley, L. W., Anderson, P. G., and Pearson, M. L., "The General Interpolants Method: A Procedure for Generating Numerical Analogs of the Conservation Laws," AIAA Paper 77-642, Albuquerque, N. Mex., June 27-28, 1977.

[10]Solomon, J. M., Ciment, M., and Ferguson, R. E., "Three-Dimensional Supersonic Inviscid Flow Field Calculations on Re-entry Vehicles with Control Surfaces," AIAA Paper 77-84, Los Angeles, Calif., Jan. 24-26, 1977.

[11]Barnwell, R. W., "A Time-Dependent Method for Calculating Supersonic Blunt-Body Flow Fields with Sharp Corners and Embedded Shock Waves," NASA TN D-6031, Nov. 1970.

[12]Ferri, A., "Supersonic Flows with Shock Waves," *High Speed Aerodynamics and Jet Propulsion: General Theory of High Speed Aerodynamics*, Vol. VI, Princeton Univ. Press, Princeton, N.J., 1954, Sec. H, pp. 704-706, 732.

[13]Oswatitsch, K., *Gas Dynamics*, Academic Press, New York, 1956, pp. 259-261, 489.

[14]Hayes, W. B. and Probstein, R. F., *Hypersonic Flow Theory: Inviscid Flows*, 2nd Ed., Vol. I, Academic Press, New York, 1966, pp. 530-531.

[15]Melnik, R. E., "Vortical Singularities in Conical Flow," *AIAA Journal*, Vol. 5, April 1967, pp. 631-637

[16]Bakker, P. G. and Bannink, W. J., "Conical Stagnation Points in the Supersonic Flow Around Slender Circular Cones at Incidence," Dept. of Aeronautical Engineering, Delft Univ. of Technology, Rept. VTH-184, Nov. 1974.

[17]Kurosaki, M., "A Study of Supersonic Conical Flow," Inst. of Space and Aeronautical Science, Univ. of Tokyo, Rept. 498, 1973.

[18]Houwink, R. and Nebbeling, C., "Experimental Investigation of the Leeward Flow Field of a Cone at High Incidence in Supersonic Flow," *Mechanical and Aeronautical Engineering and Shipbuilding*, Delft Progress Rept. Set. C., Vol. 1, 1975, pp. 69-76.

[19]Moretti, G., "Importance of Boundary Conditions in the Numerical Treatment of Hyperbolic Equations," *The Physics of Fluids*, Vol. 12, Suppl. Pt. II, Dec. 1969, pp. II13-II20.